World Academy of Science, Engineering and Technology
International Journal of Electrical and Computer Engineering
Vol:19, No:1, 2025

An Approach to Control Electric Automotive Water Pumps Deploying Artificial Neural Networks

Gabriel S. Adesina, Ruixue Cheng, Michael Short, Geetika Aggarwal

***Abstract*—**With the global shift towards sustainability and technological advancements, electric hybrid vehicles (EHVs) are increasingly being seen as viable alternatives to traditional internal combustion (IC) engine vehicles, which also require efficient cooling systems. The electric automotive water pump (AWP) has been introduced as an alternative to IC engine belt-driven pump systems. However, current control methods for AWPs typically employ fixed gain settings, which are not ideal for the varying conditions of dynamic vehicle environments, potentially leading to overheating issues. To overcome the limitations of fixed gain control, this paper proposes implementing an artificial neural network (ANN) for managing the AWP in EHVs. The proposed ANN provides an intelligent, adaptive control strategy that enhances the AWP's performance, supported through MATLAB simulation work illustrated in this paper. Comparative analysis demonstrates that the ANN-based controller surpasses conventional PID and fuzzy logic controllers (FLC), exhibiting no overshoot, 0.1 secs rapid response, and 0.0696 integral absolute error (IAE) performance. Consequently, the findings suggest that ANNs can be effectively utilized in EHVs.

***Keywords*—**Automotive water pump, cooling system, electric hybrid vehicles, artificial neural networks, PID control, fuzzy logic control, IAE, MATLAB.

I. Introduction

IN recent years, there has been a global shift towards sustainability and the advancement in technology; in response, EHVs are becoming increasingly prevalent as an alternative to conventional IC engine vehicles. This transition is driven by the urgent need to reduce greenhouse gas emissions and decrease reliance on fossil fuels. Among the critical components of any vehicle, the cooling system plays a pivotal role in maintaining the optimal operating temperature, thereby preventing overheating, and ensuring efficient performance [1]. In conventional IC engines, the cooling system is typically described as a belt-driven mechanical pump system the function of the pump is determined by the speed and torque of the engine for a cooling state to be achieved, else it will experience overheating [2].

The fundamental difference in the operational mechanisms of AWPs in EHVs compared to IC engines is that EHVs employ one or more electric AWPs for cooling dependence on electric signals for functioning and IC engines depend on torque generated by the engine. Furthermore, AWP systems offer advantages over conventional systems, including less consumption of energy for rapid cooling and less friction parts. Brushless Direct Current (BLDC) motors have been utilized by AWPs [2], to achieve overall efficiency the speed needs to be controlled robustly and efficiently.

Electromechanical systems and BLDC motors have had different control schemes implemented but limited numbers have been applied to AWPs [3]. The Proportional-Integral-Derivative (PID) is the most utilized control scheme because of how widely accepted and efficient with ease in tuning. However, despite this advantage, the dynamic nature of AWP operations in EHV systems pose challenges on the fixed gain of PID control, as EHV operational scenarios are constantly changing [4], [5].

A. Conceptual Framework

AWPs are Direct Current (DC) motor devices that convert electrical power into mechanical energy. They are extensively utilized in various industrial applications due to their wide range of variable speeds and straightforward control mechanisms. DC motors are often paired with actuators in circuits because of their continuous rotational motion and ease of control, making them ideal for applications requiring precise speed regulation [6]. The speed of a DC motor is directly proportional to the armature voltage and inversely proportional to the excitation flux. These characteristics make DC motors suitable for a wide range of manufacturing applications, including electric hoists, electromotive systems, and robotics.

The long-standing use of DC motors in manufacturing control is attributed to their numerous advantageous features, including high response, linear starting torque control, and ease of control [7]. The main specification of a DC motor is its speed, which is usually controlled by varying the supplied voltage. This versatility and reliability make DC motors a staple in the manufacturing sector for applications that require precise speed regulation.

Additionally, research by [2] delved into the design and implementation of a BLDC motor drive for AWPs. This study emphasizes the transition from conventional mechanical water pumps, which are directly connected to the engine belt and operate continuously regardless of coolant circulation, to electric water pumps, which can operate at various speeds, thereby reducing energy consumption. The BLDC motor drive designed for this application operates at a nominal voltage of 13.5 V with a rated power of 350 W and a maximum speed of 9000 rpm. Key considerations in the design include high-temperature endurance and protection against reverse voltage, ensuring reliability and efficiency in the harsh automotive environment and the motor and drive exhibited an efficiency of

Gabriel S. Adesina, Ruixue Cheng, Michael Short, and Geetika Aggarwal are with Department of Engineering SCEDT, Teesside University, Middlesbrough, England (e-mail: 2adesinagabriel@gmail.com, R.Cheng@tees.ac.uk, m.short@tees.ac.uk, G.Aggarwal@tees.ac.uk).

78%.

B. Employed Control Scheme

The control of electromechanical systems has seen significant advancements, particularly with the implementation of PID controllers. The PID controller, a staple in the control industry, is widely used due to its structural simplicity, robustness, and effectiveness in managing a broad spectrum such as robotics, Automotive systems and electromechanical in industrial applications [8]. Its popularity stems from its ability to provide reliable feedback control, which is crucial in maintaining system stability and performance across various operating conditions.

However, the limitations of PID controllers become apparent when dealing with highly dynamic systems such as electric AWPs in EHVs. The fixed-gain characteristics of PID controllers make them less adaptable to the varying operational conditions inherent in EVs, where the demand for cooling can fluctuate rapidly [4]. To address these limitations, alternative control strategies have been explored.

Several research efforts have focused on improving the control mechanisms for AWPs. In one study, employing PID and Linear Quadratic Regulation (LQR) controllers made the automotive engine cooling system electronically controlled. The outcome indicated the controllers could maintain engine coolant temperature within acceptable limits across various operating scenarios. However, it posed challenges in dynamic scenarios concerning the fixed-gain nature of these controllers [9]. Similarly, a demand-based control system was designed for efficient heat pump operations in EVs using PI (Proportional Integral) controllers. This approach reduced energy consumption, but the design of conventional PI controller is still not efficient enough [10].

Previous research by [11] has thoroughly examined Flatness-based Control (FBC) and Field-Oriented Control (FOC), two significant control strategies for electric AWPs in electric and hybrid vehicles, applied to Permanent Magnet Synchronous Motors (PMSMs). FOC employs PI controllers to regulate the stator current, thereby managing the speed and torque of PMSMs. Despite its widespread use due to its straightforward implementation and ease of tuning, FOC encounters challenges in dynamic environments because of its fixed gain characteristics, which restrict its adaptability to the varying conditions typical in electric vehicles.

In contrast, FBC leverages differential flatness theory to provide high dynamic performance and robustness against model inaccuracies and external disturbances. This method allows for direct control of the state variables and outputs of PMSMs, offering a more adaptive control mechanism compared to traditional FOC. These findings highlight the necessity for advanced control strategies in AWPs to enhance efficiency and adaptability.

Further study was done by implementing Fuzzy logic to the control scheme of electric AWPs [3] to control the gain and offer an intelligent and adaptive control strategy the FLC shows a prevalence advantage to the PID making it more efficient in the consumption of energy.

The FLC for AWPs prompted the adoption of ANNs. For instance, ANNs have been successfully applied in speed control [12], where they have demonstrated superior performance in handling nonlinear dynamics and uncertainties compared to conventional control methods.

In 2002, researchers investigated the effects of an ANN (ANN) controller on DC motor speed. The study utilized a three-layer ANN model comprising an input layer, a hidden layer with three neurons, and an output layer. However, the speed response curve obtained from this setup was not smooth, indicating limitations in the intelligent control method used [13]. This early research highlighted the potential but also the challenges of using ANNs for DC motor speed control.

Further advancements were made in 2014 when a study investigated the impact of ANN controllers on DC motor speed response. This study employed a single hidden layer with one neuron. The results revealed that the output speed response curve was unstable and failed to reach a settling state, indicating that the chosen configuration was inadequate for stable speed control [14]. These findings highlighted the necessity for more refined and robust ANN configurations to ensure reliable speed control in DC motors.

II. Reasearch Methodology

A. Electric AWP Model Development

The AWP is modeled as an electromechanical system, as described in [3]. In this model, an applied voltage (V_a) drives a current (i_t) through the motor's armature winding, encountering resistance (R) and inductance (L). The current flow generates a magnetic field, which interacts with the motor's magnetic field to produce torque (T_m), causing the rotor to turn. This rotation results in angular displacement (θ) and angular velocity (ω). As the motor operates, it generates a back electromotive force (V_b) which opposes the applied voltage and affects the current (i_t). The system experiences frictional losses, represented by the damping coefficient (B), as well as the opposing load torque (T_d). Together, these factors determine the net torque and rotational speed of the motor. The interaction between the electrical and mechanical components ensures that the motor operates efficiently, controlling the speed and torque required for the water pump's operation as illustrated in Fig. 1 and Table I, respectively.

The electric circuit of the AWP gives (1) of the sum of voltage drops:

$$V_a(t) = i_a(t)R + L\frac{di_a(t)}{dt} + V_b \quad (1)$$

Laplace Transform from (1):

$$V_a(s) = (Ls + R)I_a(s) + V_b(s) \quad (2)$$

The relationship between the back EMF and angular velocity is expressed as $V_b = K_b\omega$; where the variable ω represents the angular velocity

$$V_a(s) = (Ls + R)I_a(s) + K_b\omega(s) \quad (3)$$

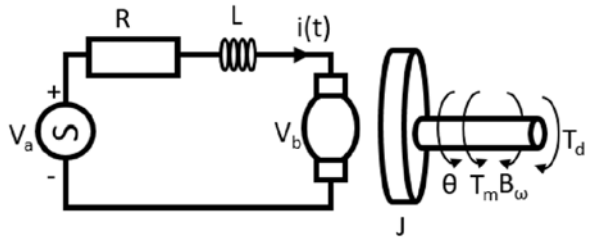

Fig. 1 An Electromechanical System

TABLE I
SYSTEM PARAMETERS OF THE AWP

Parameters	Value
Torque Constant, Kt	3.5 NM/Amp
Back EMF constant, Kb	3.5 v/rad/sec
Viscous friction coefficient, B	0.0348 MN/rad sec
Rotor Inertia, J	0.068K g/m^2
Armature Inductance, L	0.055 H
Armature Resistance, Ra	7.56 Ω

For the mechanical circuit, the torque produced by the armature current is proportional to the armature current, as shown in (4):

$$T_m(s) = K_t I_a(s) \tag{4}$$

$$K_t I_a(s) = Js\omega(s) + B\omega(s)$$

$$K_t I_a(s) = (Js + B)\omega(s)$$

$$I_a(s) = \frac{Js+B}{K_t}\omega(s) \tag{5}$$

Substituting both circuits, $I_a(s) = \frac{Js+B}{K_t}\omega(s)$ into (3):

$$V_a(s) = (Ls + R)\frac{Js+B}{K_t}\omega(s) + K_b\omega(s)$$

$$V_a(s) = ((Ls + R)\frac{Js+B}{K_t} + K_b)\omega(s) \tag{6}$$

Simplifying the transfer function:

$$V_a(s) = (\frac{LJs^2+(LB+RJ)s+RB+K_bK_t}{K_t})\omega(s)$$

$$\omega(s) = (\frac{K_t}{LJs^2+(LB+RJ)s+RB+K_bK_t})V_a(s) \tag{7}$$

$$G(s) = \frac{\omega(s)}{V_a(s)} = (\frac{K_t}{LJs^2+(LB+RJ)s+RB+K_bK_t}) \tag{8}$$

Model transfer function is obtained from (8) after inputting the values from Table I.

B. ANN Design

ANNs are sophisticated computational models designed to emulate the behavior of biological neural networks. These models are instrumental in solving complex functions across a diverse array of applications [15]. Fundamentally, ANNs are structured into three principal layers: the input layer, hidden layer(s), and output layer [16]. Each of these layers can comprise numerous computational nodes, commonly referred to as neurons, depending on the complexity and requirements of the task at hand [17]. The primary benefits of utilizing ANNs include their processing speed, simplicity, and the capacity to leverage historical data for predictive purposes. ANNs have found extensive application in fields such as pattern recognition, optimization, clustering, regression, and predictive analytics.

Training an ANN involves presenting it with various known input and corresponding desired output vectors. During this process, the weights associated with the connections between neurons are iteratively adjusted to minimize the discrepancy between the actual output produced by the ANN and the target output. This adjustment is typically carried out using optimization algorithms such as backpropagation. Training continues until the ANN achieves a predefined level of accuracy. Upon reaching this accuracy threshold, the training phase concludes, and the ANN's performance is evaluated using a separate set of data not previously encountered during training. This testing phase is crucial for validating the model's generalization capability and ensuring its effectiveness in real-world scenarios. For a more comprehensive understanding of these training and evaluation processes, refer to the detailed explanations provided in [17].

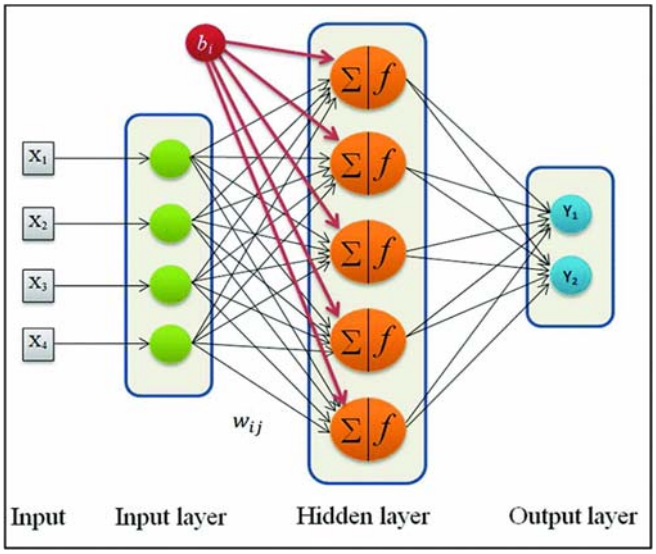

Fig. 2 The Structure of ANN

In this research, data for training the ANN were generated using a MATLAB script. The data generation process focused on an AWP model, varying several key parameters to create a comprehensive dataset. Engine temperature varied from 80 °C to 100 °C, reflecting typical operational ranges. Coolant temperature ranged between 75 °C and 95 °C, capturing the dynamic thermal management within the engine cooling system. Engine load varied from 0% to 100%, covering the full spectrum of operating conditions, from idle to maximum load. Ambient temperature was varied from -20 °C to 50 °C, covering extreme environmental conditions. These systematically

combined parameters ensured a diverse and representative dataset, providing a robust foundation for the ANN to develop accurate predictive capabilities for various operating scenarios of the AWP. Detailed methodology, including the MATLAB script, is available in the appendix, ensuring transparency and reproducibility.

The neural network (NN) was trained using MATLAB's "nnstart" toolbox, with an architecture that included four input parameters: engine temperature, coolant temperature, ambient temperature, and engine load. The structure comprised 10 hidden layers, capturing complex patterns and relationships within the data. The primary objective was to predict the speed of the AWP. The training process employed the Levenberg-Marquardt algorithm, known for its efficacy in managing non-linear problems, making it suitable for AWP systems. This algorithm uses a loss function defined as the sum of squared errors and approximates the Hessian to ensure positive definiteness. The weight parameter update rule facilitates steady progress towards the function's minimum, transitioning to rapid convergence as needed [18].

$$W_{i+1} = W_i\text{-}(J_i^T.J_i + \lambda_i.I)^{-1}.(2J_i^T.e_i);\ \mathrm{i} = 0, 1 \ldots$$

The mathematical model of the entire system was implemented in MATLAB, as depicted in Fig. 3. The network training algorithm is given in the flowchart in Fig. 4.

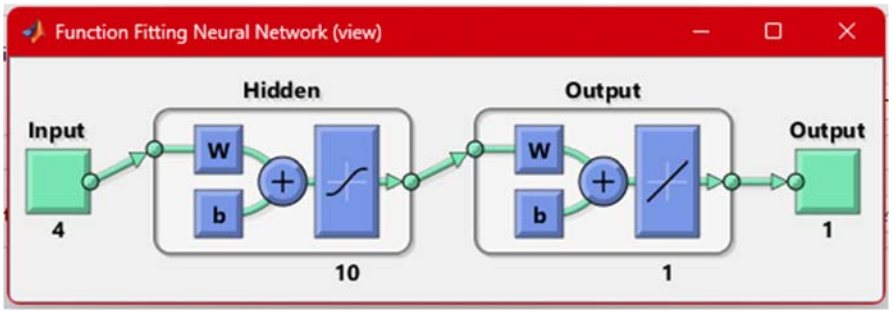

Fig. 3 ANN Training Data

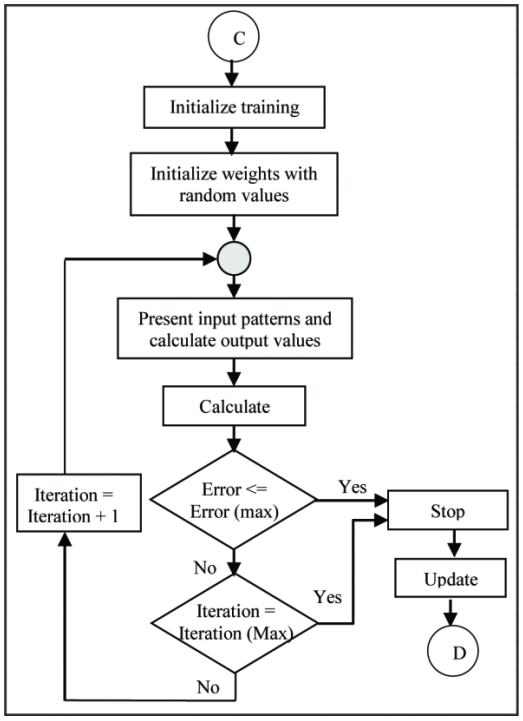

Fig. 4 Flowchart of ANN Training

The neural network, trained on the generated data summarized in Table II, completed 1000 epochs of training. This process resulted in a substantial reduction in the mean squared error (MSE) to 1.06e-08. The gradient, which initially measured 4.246e+03, decreased to 1.00e-07, indicating near-optimal training and proximity to the target value. The learning rate ('Mu') started at 0.001 and was reduced to 1.00e-10, reflecting the network's high learning efficiency. Additionally, no validation checks were necessary, as opposed to a target of 6, underscoring the model's excellent fit to the training data.

TABLE II
NN TRAINING PROGRESS METRICS

Unit	Initial Value	Stopped Value	Target Value
Epoch	0	1000	1000
Elapsed Time	-	00:00:06	-
Performance	2.64E+03	1.06E-08	0
Gradient	4.24E+03	1.57E-04	1.00E-07
Mu	0.001	1.00E-05	1.00E+10
Validation Checks	0	0	6

Fig. 5, which shows the MSE performance graph for the generated data, illustrates the training progression over epochs. Throughout 1000 epochs, the MSE decreases, achieving an optimal validation performance of 1.06e-08 by epoch 1000. This reflects a swift and effective training process. The lines representing the training, validation, and test sets converge closely, indicating the network's robust generalization capability.

Fig. 6 displays the general regression plots for the generated data, illustrating the relationship between the targets and the neural network outputs across the Test, Validation, and Training datasets. An R-value of 1 in these plots indicates perfect alignment between the network's predictions and the target values, displaying the neural network's highly accurate predictive abilities.

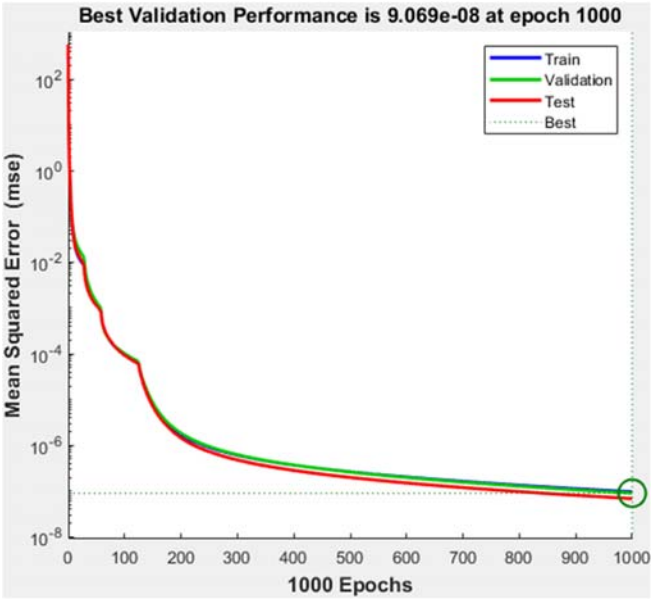

Fig. 5 Validation Performance of NN Training

III. Implementation, Result and Discussion

The modeling and simulation of the AWP were achieved using the MATLAB/Simulink (R2022b). The model was simulated with a unit step as engine temperature, alongside engine load, coolant temperature, and ambient temperature as input parameters. While the performance system was based on the transient response metrics of rise time, settling time, and Integrated Absolute Error (IAE) as the performance indices of the ANN. The Simulink diagram of the AWP ANN is shown in Fig. 7.

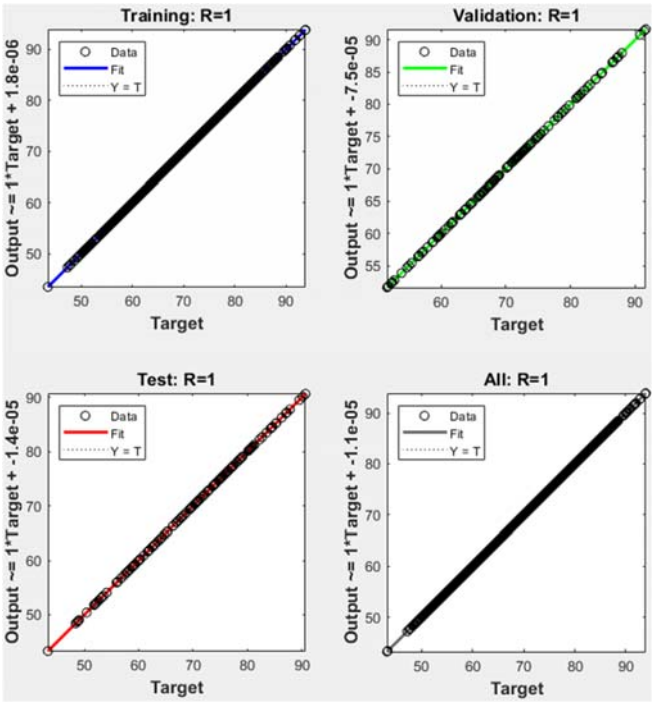

Fig. 6 Regression Plot of Trained NN

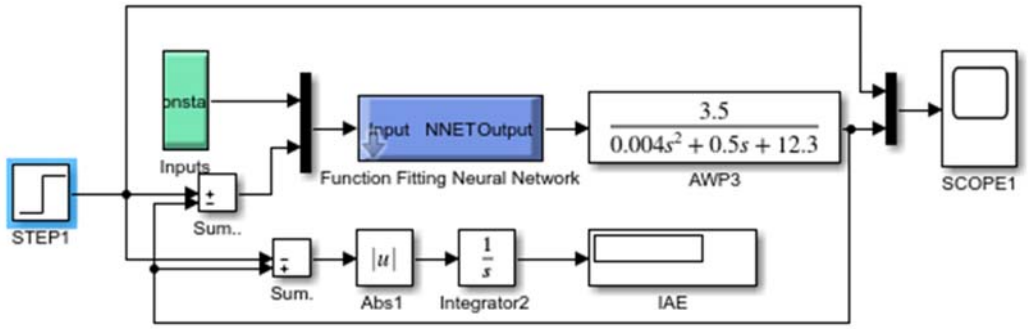

Fig. 7 Simulink Diagram of AWP ANN Controller

TABLE III
Comparison of Control System Responses

Parameters	Controllers			
	No Control	PID	FLC	ANN
Rise Time (Secs)	-	0.1	9.1	0.1
Settling Time (Secs)	-	6.7	17.7	0.3
Overshoot (%)	-	51.2	0	0
IAE	38.15	0.517	4.452	0.0696

The output signal depicted in Fig. 8 reveals that the open-loop response of the AWP exhibits undershoot behavior, failing to achieve the desired set point. A detailed analysis of the AWP's open-loop performance indicates a significant IAE, highlighting the imperative need for an advanced control strategy to enhance system performance.

Contrary to the open-loop performance, the ANN-based controller for the AWP demonstrates significant improvement in transient response. The ANN achieves a rise time of 0.1 seconds and a settling time of 0.3 seconds, with zero overshoot, which is highly desirable for AWP operation. Additionally, the ANN registers an IAE index of 0.0696. To validate the ANN's performance, comparisons were made with a FLC and a conventional PID controller, as illustrated in Fig. 6. The FLC exhibited a slower response, with a rise time of 9.1 seconds and a settling time of 17.7 seconds, while the PID controller showed a faster response, with values of 0.1 seconds for rise time and 6.7 seconds for settling time. However, the PID controller exhibited an overshoot of approximately 51.4%, which is undesirable for AWP operation. The ANN's response metrics

are superior to those of both the PID and FLC, with the PID outperforming the FLC in speed but not in overshoot control.

Table III summarized the performance of the open loop (No Control condition), the conventional PID, the FLC, and the ANN controllers. The table indicates that both the conventional PID and the ANN exhibit fast response times and low IAE values. However, the conventional PID controller experiences an overshoot exceeding 50%. The FLC shows a slower response but avoids overshoot, making it preferable to the PID in terms of stability. This suggests that while the PID controller can be utilized in applications where rapid response and performance speed are critical, it will incur significant overshoot. Conversely, the FLC is better suited for applications requiring precise set point tracking without overshoot. The ANN, however, offers an optimal solution, combining fast response, high performance speed, accuracy, and effective set point tracking. This makes it the best fit for applications requiring both rapid and precise pump control, ensuring fast and accurate pumping action.

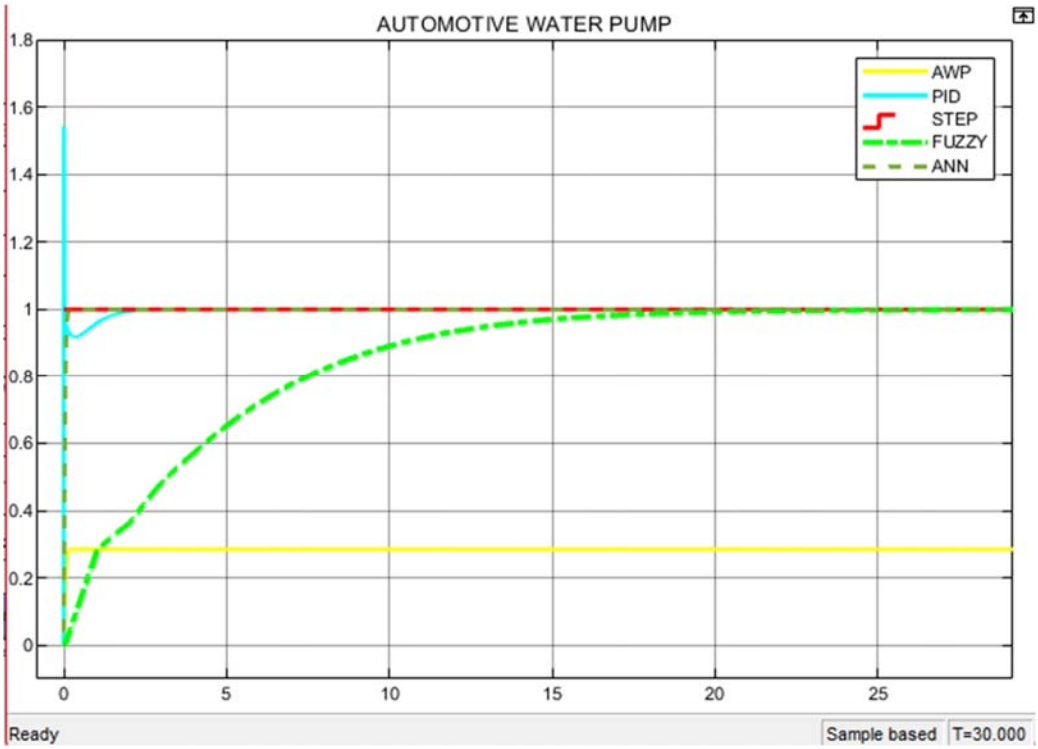

Fig. 8 Comparison of All System Responses

IV. Conclusion

In conclusion, this paper demonstrates the effectiveness of employing an ANN control strategy for Electric AWPs in EHVs. The ANN-based controller significantly outperforms conventional PID and FLC by offering rapid response, zero overshoot, and superior precision in maintaining optimal operating conditions. The ANN's adaptability to varying conditions in EHVs highlights its potential for enhancing both the performance and reliability of automotive cooling systems, making it an ideal choice for next-generation vehicle technologies. However, the real-time implementation may present challenges related to data acquisition from various geographical locations due to temperature variations and the complexities of the overall vehicle control architecture. More research can be done on genetic algorithm.

Acknowledgment

We wish to express gratitude to the institution for unwavering support through the research process.

References

[1] Liu, Y., Kang, Y., Sun, W. and Xu, X., "Power Control Strategy and Performance Evaluation of a Novel Two-pump Hydraulic Control Unit for BEVs", 2020.

[2] Joon Sung Park, B.-G. Gu, J.-H. Choi, and I.-S. Jung, "Development of BLDC Motor Drive for Automotive Water Pump Systems," *Journal of International Council on Electrical Engineering*, vol. 1, no. 4, pp. 395–399, Oct. 2011.

[3] Jibril Abdullahi Bala, Ndukwe Okpo Kalu, S. U. Hussein, and Taliha Abiodun Folorunso, "A Fuzzy Logic Control Scheme for Electric Automotive Water Pumps," *2022 IEEE Nigeria 4th International Conference on Disruptive Technologies for Sustainable Development (NIGERCON)*, Apr. 2022.

[4] Halima Yakubu, S. Thomas, S. U. Hussein, V. C. Anye, Gokhan Koyunlu, and Omotayo Oshiga, "Azimuth Position Control for Deep Space Antenna using Fuzzy Logic Controller," Dec. 2019.

[5] H. Yakubu, S. Hussein, G. Koyunlu, E. Ewang, and S. Abubakar, "Fuzzy-PID Controller for Azimuth Position Control of Deep Space Antenna," *Covenant Journal of Informatics & Communication Technology*, vol. 8, no. 1, Jun. 2020.

[6] Dakheel, H.S., Speed control of separately exited DC motor using artificial neural network. *Journal of Engineering and Sustainable Development*, *16*(4), pp.349-362. 2012.

[7] W. M. Elsrogy, M. A. Fkirin, and M. A. M. Hassan, "Speed control of DC motor using PID controller based on artificial intelligence techniques," *IEEE Xplore*, May 01, 2013.

[8] P. Mohindru, G. Sharma, and P. Pooja, "Simulation Performance of PID and Fuzzy Logic Controller for Higher Order System," *Communications on Applied Electronics*, vol. 1, no. 7, pp. 31–35, May 2015, doi: https://doi.org/10.5120/cae-1604.

[9] M. Mohamed, M. H. S. M. S. E.-D. a. M. F., Performance of Electronically Controlled Automotive Engine Cooling System Using PID and LQR Control Techniques. IOSR J. Mech. Civ. Eng., Volume 15, pp. 42-45. 2018.

[10] D. Dvorak, D. Basciotti, and I. Gellai, "Demand-Based Control Design for Efficient Heat Pump Operation of Electric Vehicles," *Energies*, vol. 13, no. 20, p. 5440, Oct. 2020.

[11] Milad Akrami, Ehsan Jamshidpour, Serge Pierfederici, and V. Frick, "Comparison of Flatness-based Control and Field-Oriented Control for PMSMs in Automotive Water Pump Application," Jun. 2023.

[12] Sofiane Ben Abdi, Abderrazak Debilou, Aicha Guergazi, Younes Samsar, and Mahdi Labed, "Speed Control of BLDC Quadrotor Motor Using an ANN Trained with PID Controller Data Optimized by PSO Algorithm," Apr. 2024.

[13] Ph. Q. Dzung, and Le. M. Phuong, "ANN-Control system dc motor". Faculty of Electrical and Electronic Engineering HCMC University of Technology Ho Chi Minh City-Vietnam *IEEE Transactions*, pp.82-90. 2002.

[14] H. Sh., "Speed Control of Separately Exited DC Motor Using Artificial Neural Network," *Journal of Engineering and Development*, vol. 16, no. 4, pp. 349–362, Jan. 2012.

[15] A. Sözen, T. Menlik, and S. Ünvar, "Determination of efficiency of flat-plate solar collectors using neural network approach," *Expert Systems with Applications*, vol. 35, no. 4, pp. 1533–1539, Nov. 2008.

[16] M. Caner, E. Gedik, and A. Keçebaş, "Investigation on thermal performance calculation of two type solar air collectors using artificial neural network," *Expert Systems with Applications*, vol. 38, no. 3, pp. 1668–1674, Mar. 2011.

[17] N. I. Santos, A. M. Said, D. E. James, and N. H. Venkatesh, "Modeling solar still production using local weather data and artificial neural networks," *Renewable Energy*, vol. 40, no. 1, pp. 71–79, Apr. 2012.

[18] S. Halder, A. Khan, Uttam Narendra Thakur, and S. Saha, "Design and Analysis of Temperature Control System using Conventional PI and Advanced ANN Controllers," *2018 International Conference on Computing, Power and Communication Technologies (GUCON)*, Sep. 2018.